# Fast Power System Analysis via Implicit Linearization of the Power Flow Manifold

Saverio Bolognani and Florian Dörfler

***Abstract*— In this paper, we consider the manifold that describes all feasible power flows in a power system as an implicit algebraic relation between nodal voltages (in polar coordinates) and nodal power injections (in rectangular coordinates). We derive the best linear approximant of such a relation around a generic solution of the power flow equations. Our linear approximant is sparse, computationally attractive, and preserves the structure of the power flow. Thanks to the full generality of this approach, the proposed linear implicit model can be used to obtain a fast approximate solution of a possibly unbalanced three phase power system, with either radial or meshed topology, and with general bus models. We demonstrate how our approximant includes standard existing linearizations, we validate the quality of the approximation via simulations on a standard testbed, and we illustrate its applicability with case studies in scenario-based optimization and cascading failures.**

## I. INTRODUCTION

Recent technological advances, together with new environmental concerns and economic goals, have driven the transition toward a new generation of power grids characterized by unprecedented challenges, such as the integration of intermittent renewable energy sources, the exploitation of distributed storage devices, the integration of large scale electric mobility, the protection against cyber-attacks, and a general requirement of higher efficiency and reliability.

In order to tackle these problems, new and advanced methodologies have been developed, including (but not limited to) distributed and robust state estimation [1], [2], detection and mitigation tools for cyber security [3], [4], distribution grid and load automation [5]. To enable the application of these methods, tractable (preferably linear), computationally efficient, and scalable, models for the power system are needed. Classical linear models available in the power systems literature fall short, either because they rely on some simplifying assumptions that diminish they descriptiveness, or because they fail to exhibit some of the desired qualities that we have mentioned. Finally, due to the growing system volatility, power grids are increasingly operated far away from the operating points [6], which renders the conventional power flow approximations ineffective.

We approach this challenge based on two key ideas.

First, we consider power grid equations without bus models, i.e., we consider all power injections and voltages that are compatible with the network physics independent of bus models such as PV, PQ, or slack buses. In many applications, such as state estimation, learning, and monitoring/fault detection, such a physical relation is everything that is needed.

Second, we aim at an implicit model, i.e., a model in the form $F(x) = \mathbb{0}$. In this form, the physical relation precedes the choice of "inputs" and "outputs" similar to the notion of behavioral systems [7]. In the vast majority of applications, having an implicit model is not a disadvantage. On the other hand, this choice allows to obtain a model which is sparse (thus computationally attractive) and structure preserving.

The original contribution of the paper will be presented as follows. In Section II we define the *power flow manifold* that describes the set of feasible power flows on a grid. In Section III we show how an implicit linear approximation for the power flow manifold can be obtained via geometric methods. We also illustrate how the proposed model generalizes all standard linear power flow models, including polar/rectangular DC power flow and their variations [8]–[12] as well as LinDistFlow [13]–[15], how to assess and improve its approximation accuracy, and how to extend it to three-phase networks. In Section IV we show how to use the approximation of the power flow manifold to solve a power flow analysis problem, where bus loads are introduced (the MatLab/GNU Octave code is available in a public online repository [16]). In Section V we review some applications where the features of the proposed model are fruitfully exploited. Finally, Section VI concludes the paper.

## II. THE POWER FLOW MANIFOLD

We define the following quantities for each bus $h$ of an $n$-bus power network:[1]

- complex voltage $u_h = v_h e^{j\theta_h} \in \mathbb{C}$, where $v_h, \theta_h \in \mathbb{R}$,
- injected complex power $s_h = p_h + jq_h \in \mathbb{C}$, where $p_h, q_h \in \mathbb{R}$.

In the following, we drop the subscript $h$ whenever we refer to the vector obtained by stacking the scalar nodal quantities, for $h = 1, \dots, n$. Let us also define the *nodal admittance matrix* $Y \in \mathbb{C}^{n\times n}$ via its elements

$$Y_{hk} = \begin{cases} y_h^{\text{sh}} + \sum_{\ell \neq h} y_{h\ell} & \text{if } k = h \\ -y_{hk} & \text{otherwise} \end{cases}$$

where $y_{hk}$ is the admittance of the power line directly connecting bus $h$ and bus $k$, and $y_h^{\text{sh}}$ is the shunt admittance (admittance to ground) at bus $h$.

This research is supported by ETH start-up funds and the SNF Assistant Professor Energy Grant #160573. The authors are with the Automatic Control Laboratory, Swiss Federal Institute of Technology (ETH) Zürich, Switzerland. {bsaverio,dorfler}@ethz.ch

[1] In order to keep the presentation concise, a balanced symmetric network is first considered. The extension to three-phase unbalanced networks is presented in Section III-E.

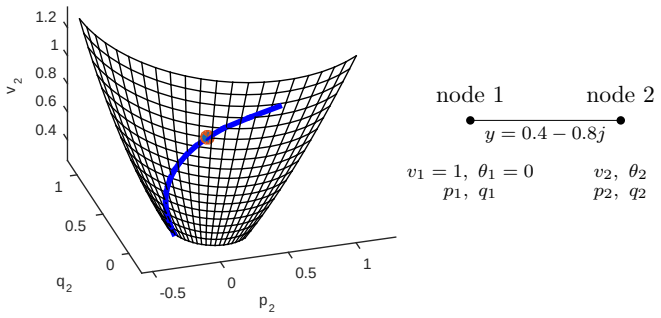


Fig. 1. Example of the *power flow manifold* $F(x) = 0$, $F : \mathbb{R}^8 \to \mathbb{R}^4$ for a two-bus network. Fixing $v_1 = 1, \theta_1 = 0$ we obtain a manifold of dimension 2, that we can represent graphically. The red dot corresponds to the no-load operating point, where $p_2 = q_2 = 0$. The thick blue curve represents the typical nose curve, with no reactive load.

The following set of nonlinear and complex-valued power flow equations descends directly from Kirchhoff's and Ohm's laws and thus need to be satisfied by any feasible power flow:

$$\operatorname{diag}(u)\overline{Yu} = s. \tag{1}$$

Let us define by $x \in \mathbb{R}^{4n}$ the grid state

$$x = (v, \theta, p, q), \tag{2}$$

and let us rewrite (1) in implicit form as $F(x) = \mathbb{0}_{2n}$, where $F : \mathbb{R}^{4n} \to \mathbb{R}^{2n}$ is obtained by expressing the complex equations (1) in real and imaginary coordinates. As the following result states, the constraint $F(x) = \mathbb{0}_{2n}$ implicitly defines a manifold

$$\mathcal{M} := \{x \,|\, F(x) = \mathbb{0}_{2n}\} \tag{3}$$

in the ambient space $\mathbb{R}^{4n}$ of voltages and injections.

**Lemma 1** (Submanifold property)**.** *The power flow manifold $\mathcal{M}$ given in* (3) *is a regular submanifold of $\mathbb{R}^{4n}$ of dimension equal to $2n$.*

The proof of Lemma 1 is available in the Appendix. Lemma 1 is not just a mere technicality but it allows us to attach a tangent plane to every point of $\mathcal{M}$, which is how we derive the best linear approximant in Section III.

Notice that we have not assumed any specific model for the buses of the grid, such as the prototypical PV, PQ, or slack buses. The *power flow manifold* (3) represents all the voltages and power injections that are compatible with the physics and yield a feasible power flow; see Figure 1.

## III. LINEAR MANIFOLD APPROXIMANT

### A. General linear approximant

In the following proposition, we derive a linear local approximant for the manifold $\mathcal{M}$ of all feasible power flows. Recall that the best linear approximant at a point $x^* \in \mathcal{M}$ is the tangent plane at $x^*$ (see Figure 2). We will explicitly construct the tangent plane in the following proposition.

**Proposition 1** (Implicit linear approximant)**.** *Let $x^* = (v^*, \theta^*, p^*, q^*)$ be a point in $\mathcal{M}$, i.e. $F(x^*) = \mathbb{0}_{2n}$. The linear manifold tangent to $\mathcal{M}$ in $x^*$ is given by*

$$A_{x^*}(x - x^*) = \mathbb{0}_{2n} \tag{4}$$

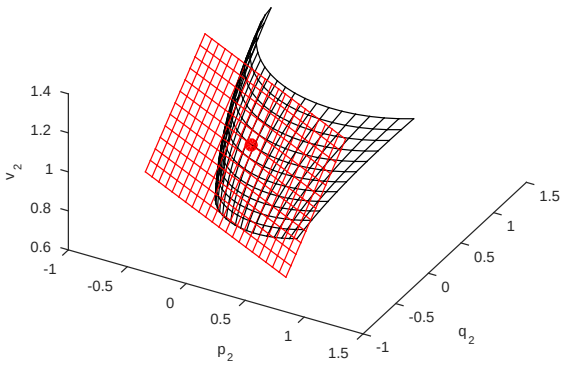


Fig. 2. Illustration of the tangent linear manifold for the two-bus example introduced in Figure 1. The red dot represents the linearization point (in this case, the no-load condition).

*with*

$$A_{x^*} = \begin{bmatrix} \Big( \langle \operatorname{diag} \overline{Yu^*} \rangle + \langle \operatorname{diag} u^* \rangle N \langle Y \rangle \Big) R(u*) & -I \end{bmatrix}, \tag{5}$$

*where*

$$\begin{aligned} u^* &:= v^* e^{j\theta^*} \\ N &:= \begin{bmatrix} I_{n\times n} & \mathbb{0}_{n\times n} \\ \mathbb{0}_{n\times n} & -I_{n\times n} \end{bmatrix} \\ \langle A \rangle &:= \begin{bmatrix} \operatorname{Re} A & -\operatorname{Im} A \\ \operatorname{Im} A & \operatorname{Re} A \end{bmatrix} \\ R(u) &:= \begin{bmatrix} \operatorname{diag}(\cos\theta) & -\operatorname{diag}(v)\operatorname{diag}(\sin\theta) \\ \operatorname{diag}(\sin\theta) & \operatorname{diag}(v)\operatorname{diag}(\cos\theta) \end{bmatrix}. \end{aligned}$$

The proof of Proposition 1 is available in the Appendix, where we also include nodal currents among the explicit system states, in order to simplify the use of the model for certain applications, e.g, evaluation of thermal limits and protection mechanisms.

The linear and implicit approximant (4) exhibits some relevant features.

**Sparsity** – Regardless of the linearization point $x^*$, the matrix $A_{x^*}$ maintains a sparse structure, with a sparsity pattern that descends directly from the network topology. This sparsity, together with the linearity, makes the approximant (4) appealing for applications with high computational burden, such as scenario-based optimization approaches, Monte Carlo simulations, cascading failures, learning methods, state estimation, and bad-data detection — to mention only a few.

**Structure-preserving** – In addition to being sparse, the approximant preserves locality of the parameters, i.e. each row of $A_{x^*}$ that involves quantities of bus $h$, only contains grid parameters (admittances) from the neighborhood of $h$. Such a structure-preserving model is a key requirement for developing methods for decentralized or distributed control, optimization, estimation, and identification.

**Geometric methods** – Geometric control or optimization methods explicitly require knowledge of the tangent plane in the current state of the grid, since the resulting control laws or iterative optimization algorithms must induce a vector field on such a tangent plane to be compatible with the physics.

Finally, it is to be said that having an implicit model is never a disadvantage. Indeed, it is of course possible to use this approximant to derive an approximate solution of the power flow equations, by completing it with appropriate bus models (as detailed in Section IV). However, this is often unnecessary; the linear manifold approximant can also be used directly in some control design and estimation problems that do not require the solution of the power flow equations, as shown in the examples in Section V.

### B. Approximation quality

As indicated in Figure 2, the approximation quality depends on the curvature of the power flow manifold, and can therefore be put in direct relationship with the second derivatives of the nonlinear equations in $F(x)$.

To see this, let us define the *power injection error* $\epsilon_i(x)$ as the $i$-th row of $F(x)$, i.e. $\epsilon_i = F_i(x)$. The name derives from the fact that $\epsilon$ is, dimensionally speaking, a power flow, and has a straightforward interpretation in terms of difference between the injected power in a bus and the power flows on the lines that leave the node. Observe that for a point $x \in \mathcal{M}$ on the power flow manifold, $F(x) = \mathbb{0}_{2n}$ and the power injection error is zero, whereas for a point $x$ on the approximant (4), we have generally a nonzero power injection error: $F_i(x) = \epsilon_i$. The following result relates the power injection error to the curvature of the manifold.

**Proposition 2** (Approximation quality)**.** *Consider a point $x^* \in \mathcal{M}$ on the power flow manifold and the linear approximant* (4) *in Proposition 1. Consider a ball $\mathcal{B}(x^*, \delta)$ of radius $\delta > 0$ around $x^*$. Then, for any $x$ in $\mathcal{B}(x^*, \delta)$ that belongs to the linear approximant, we have that for any $i$*

$$|\epsilon_i| \leq \frac{B_i}{2} \|x - x^*\|^2, \tag{6}$$

*where $B_i$ is a real number such that*

$$\left\| \frac{\partial^2 F_i}{\partial x^2} \right\| \leq B_i \qquad \forall x \in \mathcal{B}(x^*, \delta).$$

The proof of Proposition 2 is available in the Appendix.

Besides providing a convenient way to derive numerical guarantees on the quality of the approximation, this bound motivates a pre-conditioning approach that has the potential to improve the proposed model, as detailed in Section III-D.

### C. Linearization around the flat voltage solution

In order to derive the parameters $A_{x^*}$ of the proposed linear approximant, a state $x^*$ corresponding to a feasible power flow is necessary. In practical terms, and depending on the application, this can be obtained

- by numerically solving a power flow analysis problem with the grid equations (1);
- by gathering field measurements from the grid;
- by choosing a linearization point for which an analytic solution is available, for example, the *flat voltage* solution where $u = \mathbb{1} \in \mathbb{C}^n$.

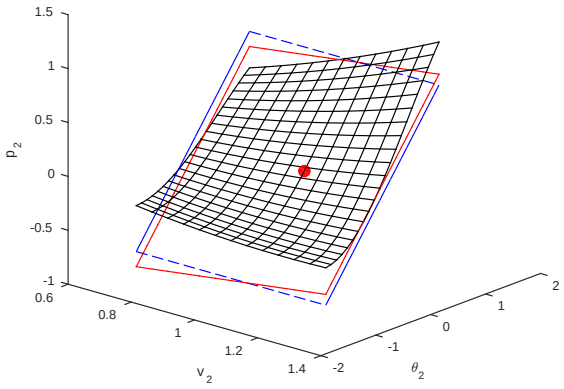


Fig. 3. Comparison of the DC power flow model (in dashed blue) with the proposed linear approximant (in solid red), for the two-bus example introduced in Figure 1. The mesh has been removed to improve readability. Compared to the best approximant tangent plane, which in this case corresponds to the kernel of $A_{\text{LC}}$, the heuristic $A_{\text{DC}}$ is a rotation thereof, and fails at modeling the relation between active power and voltage magnitudes.

Indeed in the latter case, notice that $\operatorname{diag}(\mathbb{1})Y\mathbb{1} = y^{\text{sh}}$, where $y^{\text{sh}} \in \mathbb{C}^n$ is the vector of nodal shunt admittances. Hence, $u = \mathbb{1}_n \in \mathbb{C}^n$ and $s = y^{\text{sh}}$ is a solution to the power flow equations: $F(\mathbb{1}_n, \mathbb{0}_n, \operatorname{Re} y^{\text{sh}}, \operatorname{Im} y^{\text{sh}}) = \mathbb{0}_{2n}$.

By using the fact that $R(\mathbb{1}) = I_{2n \times 2n}$, the linear approximation matrix in (4) reduces to

$$A_{\text{flat}} = \begin{bmatrix} \langle \operatorname{diag} \overline{y^{\text{sh}}} \rangle + N \langle Y \rangle & -I \end{bmatrix}. \tag{7}$$

Previously proposed approximations can be derived from the linearization matrix (7) corresponding to the flat voltage profile. For example, by assuming zero shunt admittances ($y^{\text{sh}} = 0$), one obtains

$$A_{\text{LC}} = \begin{bmatrix} \operatorname{Re} Y & -\operatorname{Im} Y & -I & 0 \\ -\operatorname{Im} Y & -\operatorname{Re} Y & 0 & -I \end{bmatrix},$$

which equals the *Linear Coupled power flow model* proposed in [8, (25)-(26)] and in [9, (15)] in rectangular coordinates.

$$A_{\text{LC}}(x - x^*) = \mathbb{0}_{2n} \;\Leftrightarrow\; \begin{bmatrix} \operatorname{Re} Y & -\operatorname{Im} Y \\ -\operatorname{Im} Y & -\operatorname{Re} Y \end{bmatrix} \begin{bmatrix} v \\ \theta \end{bmatrix} = \begin{bmatrix} p \\ q \end{bmatrix}.$$

Also, by also assuming purely inductive lines ($\operatorname{Re} Y = 0$), one obtains

$$A_{\text{DC}} = \begin{bmatrix} 0 & -\operatorname{Im} Y & -I & 0 \\ -\operatorname{Im} Y & 0 & 0 & -I \end{bmatrix},$$

which equals the *DC power flow* model [11] for the active power and a corresponding linear DC model for the reactive power and voltage [12]:

$$-\operatorname{Im} Y \theta = p, \qquad -\operatorname{Im} Y v = q.$$

A graphical comparison of the DC power flow model with the proposed linear approximant is provided in Figure 3.

Finally, when expressing the voltages in rectangular coordinates $(\operatorname{Re} u\,, \operatorname{Im} u)$, then the flat voltage linearization (7) corresponds to a recently proposed *rectangular DC power flow* model obtained by fixed-point arguments in [10].

By choosing the special linearization point $u^* = \mathbb{1}$, and by introducing a number of further assumptions on the grid parameters, we have therefore recovered most of the linear power flow models proposed in the literature. One notable exception is mentioned in the next section.

### D. Linearization after nonlinear change of coordinates

Let us define an element-wise (thus structure-preserving) smooth coordinate transformation of the state variables

$$\tilde{v}_h = \tilde{v}_h(v_h),\ \tilde{\theta}_h = \tilde{\theta}_h(\theta_h),\ \tilde{p}_h = \tilde{p}_h(p_h),\ \tilde{q}_h = \tilde{q}_h(q_h),$$

which satisfy some properties (for $\tilde{v}_h$, and equivalently for the other coordinates) that will be convenient later on:

$$\tilde{v}_h(v_h^*) = v_h^*, \qquad \frac{\partial \tilde{v}_h}{\partial v_h}(v_h^*) = 1. \tag{8}$$

Assume that the functions $\tilde{v}_h$ are invertible in the domain of interest. With a slight abuse of notation, we denote the inverse state transformation as $x = x(\tilde{x})$. The manifold of feasible power flows is therefore equivalently described by

$$G(\tilde{x}) := F(x(\tilde{x})) = 0.$$

Because of condition (8), the approximating tangent space for both $G$ and $F$ is the *same* since

$$\frac{\partial G}{\partial \tilde{x}} = \frac{\partial F}{\partial x} \cdot \frac{\partial \tilde{x}}{\partial x} = \frac{\partial F}{\partial x}.$$

However, the curvature of the manifold $G(\tilde{x}) = \mathbb{0}_{2n}$ in the neighborhood of $x^*$ depends on the specific transformation. In fact, for each row $i$ of $G$, the diagonal terms of the Hessian are affected as

$$\frac{\partial^2 G_i}{\partial \tilde{x}_j^2} = \frac{\partial^2 F_i}{\partial x_j^2} + \frac{\partial F_i}{\partial x_j} \frac{\partial^2 x_j}{\partial \tilde{x}_j^2},$$

while the off-diagonal terms remain the same:

$$\frac{\partial^2 G_i}{\partial \tilde{x}_j \partial \tilde{x}_k} = \frac{\partial^2 F_i}{\partial x_j \partial x_k} \frac{\partial x_j}{\partial \tilde{x}_j} \frac{\partial x_k}{\partial \tilde{x}_k} = \frac{\partial^2 F_i}{\partial x_j \partial x_k}.$$

Hence, by the reasoning in Section III-B, the quality of the approximation via the linear manifold $A_{x^*}(x - x^*) = \mathbb{0}_{2n}$ can be improved by a cleverly chosen transformation.

Since the power flow equations (1) are purely quadratic in the voltage magnitudes, a reasonable transformation is

$$\tilde{v}_h = v_h^2/2,\ \tilde{\theta}_h = \theta_h,\ \tilde{p}_h = p_h,\ \tilde{q}_h = q_h. \tag{9}$$

By assuming zero shunt admittances, and by adopting the flat voltage profile as linearization point, as in Section III-C, one obtains the linear implicit model

$$\begin{bmatrix} \operatorname{Re} Y & -\operatorname{Im} Y & -I & 0 \\ -\operatorname{Im} Y & -\operatorname{Re} Y & 0 & -I \end{bmatrix} \begin{bmatrix} \tilde{v} \\ \theta \\ p \\ q \end{bmatrix} = \mathbb{0}_{2n}, \tag{10}$$

where $\tilde{v}_h = v_h^2/2$ is the transformed voltage coordinate.

Interestingly, the model (10) equals the *Simplified DistFlow* model proposed in [13] (and called LinDistFlow in [17]), which however was derived for radial networks – allowing a straightforward elimination of the voltage angles $\theta$ from the state variables, see [14], [15] for recent expositions.

A comparison of the two linear approximants in Figure 4, displayed in original $v$-coordinates, shows as the nonlinear transformation seems to improve the quality of the linear approximant. Essentially, the transformation (9) and the subsequent linearization can be understood as a second-order approximation that locally matches, at least along the voltage coordinate $v_2$, the curvature of the power flow manifold.

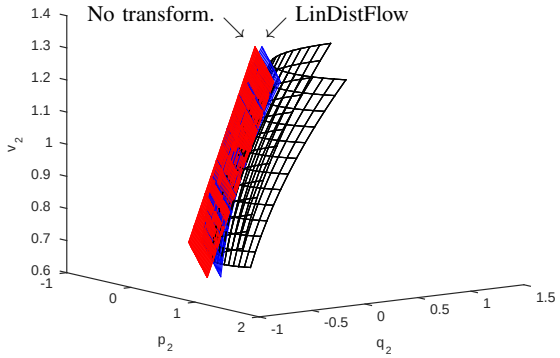


Fig. 4. Comparison of the linear approximants obtained by applying Proposition 1 to the original state variables (in red) and to their nonlinear transformation as suggested by the LinDistFlow model (10) (in blue).

Future investigation will explore the possibility of using this degree of freedom (the choice of the nonlinear transformations preceding the linearization step) in order to derive better linear approximants in different coordinates to minimize the approximation error (6).

### E. The three-phase case

The same approach adopted to obtain Proposition 1 can be replicated, in a very similar manner, to derive a linearized model for an unbalanced three-phase grid. It is sufficient to augment the notation by defining the three phase voltage at bus $h$ as

$$u_h = [u_h^a\ u_h^b\ u_h^c]^T \in \mathbb{C}^3,$$

where $u_h^a \in \mathbb{C}$ is the voltage of phase $a$ at bus $h$, with respect to ground. Similarly, we redefine $\theta$, $p$, $q$.

Each element of the admittance matrix $Y$ is now replaced by a $3 \times 3$ block. The analysis follows the same step as the single-phase case, and the result in Proposition 1 holds true. We omit the analogous but cumbersome formulae here.

As a particular example, if we assume zero shunt admittances and adopt the flat and balanced voltage profile

$$u^* = \mathbb{1} \otimes \begin{bmatrix} 0 \\ -2\pi/3 \\ 2\pi/3 \end{bmatrix}$$

as linearization point, then we obtain

$$A_{\text{flat,3-phase}} = \begin{bmatrix} N\langle \Phi^{-1} Y \Phi \rangle & -I \end{bmatrix},$$

where

$$\Phi := \operatorname{diag}\left( \mathbb{1} \otimes \begin{bmatrix} 1 \\ a \\ a^2 \end{bmatrix} \right), \qquad a := e^{-j2\pi/3},$$

and where we used the fact that $\langle \operatorname{diag} u^* \rangle = R(u^*) = \langle \Phi \rangle$ and that $\langle \Phi \rangle N = N \langle \Phi^{-1} \rangle$.

**Remark 1.** *If the network is symmetric but the power flow is possibly unbalanced, then the block $N\langle \Phi^{-1} Y \Phi \rangle$ in $A_{flat}$ is a matrix of circulant blocks. Circulant blocks are diagonalized by the Discrete Fourier Transform matrix, which in principle allows for a faster solution of the corresponding system of linear equations [18]. Although we haven't explored this*

*possibility in this paper, it is interesting to notice how the resulting diagonalized model corresponds in spirit to the classical method of* symmetrical components *for the analysis of unbalanced power systems [19].*

## IV. LINEARIZED POWER FLOW ANALYSIS

The linear approximant (4) of the manifold of feasible power flows (3) can be used in order to derive an approximate solution to a power flow analysis problem. To do so, we introduce the following standard models for the buses of the grid. For each bus $h$ we consider the implicit relation

$$g_h(x_h) = \mathbb{0}_2\,, \tag{11}$$

where $g_h : \mathbb{R}^4 \to \mathbb{R}^2$ describes the steady state behavior of the bus and specifies the fixed and free variables. The common models typically include (but are not limited to)

- PQ buses
$$g_h(x_h) = \begin{bmatrix} p_h - P_h \\ q_h - Q_h \end{bmatrix} = \mathbb{0}_2$$
- PV buses
$$g_h(x_h) = \begin{bmatrix} p_h - P_h \\ v_h - V_h \end{bmatrix} = \mathbb{0}_2$$
- slack bus
$$g_h(x_h) = \begin{bmatrix} v_h - V_h \\ \theta_h \end{bmatrix} = \mathbb{0}_2$$
- exponential loads
$$g_h(x_h) = \begin{bmatrix} p_h - P_h v_h^{\alpha_h} \\ q_h - Q_h v_h^{\beta_h} \end{bmatrix} = \mathbb{0}_2.$$

Likewise, if certain quantities are known by direct measurements, then those can be considered as fixed quantities in an analogous fashion; see Section V-B for an example. By stacking all the implicit functions $g_h(x_h)$ we obtain the constraint $G(x) = \mathbb{0}_{2n}$, where $G : \mathbb{R}^{4n} \to \mathbb{R}^{2n}$.

Adopting the same linearization point $x^*$ as in Proposition 1, let us consider the tangent linear manifold to the (possibly nonlinear) manifold $G(x) = 0$:

$$C_{x^*}(x - x^*) = d_{x^*}$$

where

$$C_{x^*} := \left.\frac{\partial G}{\partial x}\right|_{x^*}, \qquad d_{x^*} := -G(x^*). \tag{12}$$

This directly returns the following approximate power flow, as a solution of a sparse system of linear equations.

---

**First-order AC power flow solution**

Let the state $x$ of the grid be defined as in (2), and let $x^*$ be a state that satisfies the nonlinear grid equations (1).

Then a first-order approximation $\hat{x}$ of the state $x$ that solves (1) together with the bus models (11), is given by the implicit relation

$$\begin{bmatrix} A_{x^*} \\ C_{x^*} \end{bmatrix} (\hat{x} - x^*) = \begin{bmatrix} 0 \\ d_{x^*} \end{bmatrix} \tag{13}$$

where $A_{x^*}$,$C_{x^*}$, and $d_{x^*}$ are defined in (5) and (12).

---

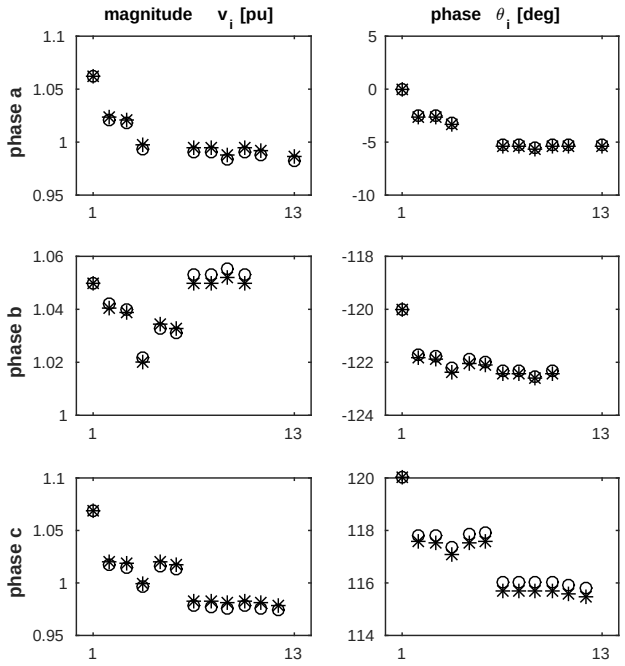


Fig. 5. Comparison of first-order AC power flow solution proposed in Section IV (stars), with the true state of the IEEE 13 test feeder (circles). Voltage magnitudes and angles are plotted for all the three phases. Missing markers correspond to missing phases in some nodes.

A numerical validation of the quality of the approximation is reported in Figure 5, based on the IEEE 13 test feeder [20], a small distribution grid which is relatively highly loaded, exhibits overhead and underground lines, shunt capacitors, and unbalanced loading. It can be observed that the approximation (13) (centered around the flat voltage power flow solution) is indeed highly accurate despite the high loading and the unbalanced nature of the grid.

For the reader's convenience we provide the MatLab/GNU Octave source code to generate the approximation (13) for a three-phase system as well as the example in Figure 5 in the online repository [16]:

`https://github.com/saveriob/1ACPF`

## V. APPLICATIONS

In this section, we briefly review some possible applications of the proposed approach, in order to illustrate its potential use and to highlight its prominent features.

### A. Scenario based decision-making in distribution networks

As a first application, taken from [21], we consider a distribution network with intermittent renewable-based microgeneration and fluctuating loads. The operator aims at maintaining the state $x$ in a feasible region $\mathcal{X}$ (defined for example by under/over voltage limits) by controlling a relatively small number of actuators, such as reactive power compensators, tap changers, and so on.

Let us define by $x^{\text{exo}}$ the components of the state $x$ that are directly driven by exogeneous factors (e.g., power injections of loads and microgenerators), and by $x^{\text{dec}}$ the

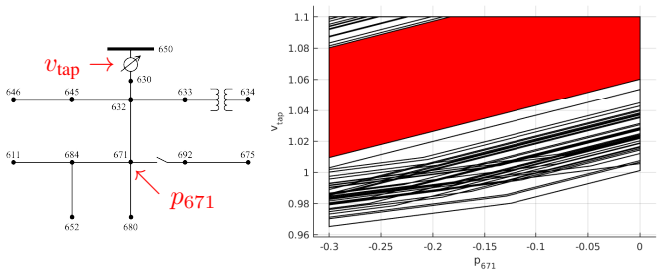


Fig. 6. Example of the feasible region computed according to the method proposed in Section V-A. In this example, the decision variables are the power injection of a curtailable microgenerator, and the voltage level of the tap changer. $M = 362$ feasible regions had to be computed and intersected in order to obtain a confidence level of 95%, resulting in a feasible region (in red) that is described by just 5 linear inequalities.

components that the distribution operator can directly control (e.g., injection of the reactive power compensators).

Assuming that the operator can derive or learn a probability distribution for $x^{\text{exo}}$, we formulate the chance-constrained decision problem of selecting $x^{\text{dec}} = \delta$ such that

$$\text{Prob}_\eta \left[ x \in \mathcal{X} \;\middle|\; \begin{array}{c} x^{\text{dec}}=\delta \\ x^{\text{exo}}=\eta \\ F(x)=0 \end{array} \right] \geq 1 - \epsilon. \tag{14}$$

The explicit computation of the set of decisions $\delta$ where this is satisfied is generally hopeless, due to the general probability distribution of the disturbances and to the nonlinear nature of both the power flow equations and the constraints. We therefore adopt the *scenario approach* [22], in which the chance-constraint (14) is replaced by a *sufficiently large* number $M$ of deterministic constraints, obtained by generating $M$ samples $\eta^{(i)}$ of the stochastic disturbance $x^{\text{exo}}$. By adopting the linear approximant proposed in Section III, and by expressing the feasible set $\mathcal{X}$ as $\{Vx \leq w\}$, the set of feasible decisions becomes the intersection of $M$ polytopes

$$\bigcap_{i=1,\ldots,M} \left\{ \delta \;\middle|\; \begin{array}{c} x^{\text{dec}}=\delta \\ x^{\text{exo}}=\eta^{(i)} \\ A_{x^*}(x-x^*)=0 \\ Vx \leq w \end{array} \right\}.$$

This approach allows to employ fast computational methods for this otherwise intractable problem, and returns a compact representation via a minimal set of linear inequalities (Figure 6). We remark that this approach critically hinges upon the computational tractability of the sparse and linear (et accurate) model (13). We refer to [21] for further details.

### B. Fault / energy theft detection

As second application of the linear implicit model (4), we focus on a state estimation and detection problem. Consider a distribution grid equipped via a metering/measurement infrastructure. We model the measured data $y$ at time $k$ as

$$y(k) = Hx(k) + \epsilon(k) + d(k), \quad k = 1, \ldots, K,$$

where $H$ is the measurement matrix, $\epsilon(k)$ is measurement noise, and $d(k)$ is an error term that could model sensor failures, cyber attacks, or energy theft via meter tampering.

We consider the problem of jointly computing estimates $\hat{d}(k)$ and $\hat{x}(k)$ of the attack vector $d(k)$ and of the state $x(k)$, such that $F(\hat{x}) = \mathbb{0}_{2n}$, given the measurements $\{y(k)\}_{k=1}^{K}$.

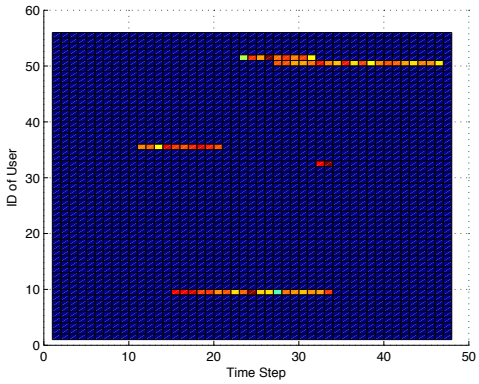


Fig. 7. In this simulations, the smart meter of 56 consumers in a power distribution network are monitored in order to identify energy theft. A relatively short sequence of 48 samples is collected, and (15) is solved numerically. The matrix $D$ is represented above (zero elements in dark blue). Because low rank of $D$ is promoted, the algorithm returns a candidate solution where few users report false measurements, for long time intervals.

The preliminary results in [23] show how, by approximating the power flow equations $F(\hat{x}) = \mathbb{0}_{2n}$ with the linear equality $A_{x^*}(x - x^*) = \mathbb{0}_{2n}$, it is possible to tackle the problem as a tractable optimization program in the form

$$\begin{aligned} \min_{D,X} \quad & \|Y - HX - D\|_2^2 + \gamma \|D\|_* \\ \text{subject to} \quad & A_{x^*}(x - x^*) = 0. \end{aligned} \tag{15}$$

where $Y, X$, and $D$ are $n \times K$ matrices that contains all time samples of $y, x$, and $d$, respectively. The last term with the nuclear norm $\|D\|_*$ is intended to promote a low rank $D$, corresponding to the more likely scenario of few attackers (or faults) acting at the same time in the grid.

The simulation results in [23] show that, using the linear approximant for the power flow manifold, it is possible to identify attacks even with relatively few samples, and measurements of only voltage magnitudes and active power (see Figure 7). We remark that these results could not have been attained with a DC power flow model neglecting voltage magnitudes and their coupling to active power. Finally, observe that for an optimization problem with power flow equations as in (15), a set of sparse and implicit constraints may actually be preferable to explicit yet dense linear equations, as obtained by a standard power flow linearization.

### C. Randomized simulation of cascading failures

As a third application, we consider the problem of simulating cascading failures in a large-scale power system, where the cascade is triggered by a localized fault and propagates because of the overloading of transmission lines [24]. Large-scale randomized simulations allow to assess the probability of this cascading phenomenon, and the impact in terms of size of the resulting blackout [25]. Due to the large number of simulations needed in this approach, approximate fast solvers of the power flow equations are typically employed, and in most cases the DC power flow model is adopted.

Our preliminary results in ongoing work [26] show that by using the first-order AC model proposed in Section IV, it is possible to obtain significantly more accurate results at the

expense of a minimal increase in the computational effort. In particular, the proposed first-order AC model properly includes the important effect of post-fault reactive power flows on the line overloading, a phenomenon that is neglected in the DC power flow approach. Furthermore, voltage constraints and under-voltage load shedding can be incorporated as well. As a result, we observe actually quite different (and much more accurate) cascading paths compared to a DC power flow model, which appears to be overly optimistic.

Again, these results critically rely upon the computational tractability and accuracy of our power flow approximation (13), and they will be detailed in a forthcoming submission.

### D. Iterative optimization over the power flow manifold

In this final application, we interpret an optimal power flow problem as an optimization problem where the decision variable is the state $x$, and the solution is constrained to belong to the power flow manifold $\mathcal{M}$ as defined in (3). We therefore have, in full generality, a program of the form

$$\text{minimize}_{x\in\mathcal{M}}\ J(x)$$

where $J(x)$ is the objective, and (for simplicity of presentation) we removed any constraints aside from the power flow equations $x \in \mathcal{M}$. Formulated in this way (where the model for individual buses is not yet specified), an optimal power flow problem is an instance of optimization over a manifold, for which iterative methods have been derived [27] and recently improved for numerical implementability [28].

In order to implement these methods, it is required to be able to produce state trajectories that remain on the manifold, and therefore a tractable formulation of the linear tangent manifold is needed. Based on the results proposed in this paper, we therefore consider an iterative approach based on the alternation of two stages, as illustrated in Figure 8.

First, the gradient of the cost function in the ambient space is projected to the linear space that is tangent to the manifold in the current operating point. By exploiting the sparse and structure-preserving properties of the approximant derived in Section III, this step can be completed in a distributed fashion by the agents in the grid. The update vector along the tangent manifold is then translated into updates for the set points of the agents, e.g., for their active power injections.

In a second stage, the physical system is actuated according to these set points, and reaches a new steady state operating point. By including the physical system in this feedback loop, we do not have to solve the power flow equations, and the operating point for the next iteration can be obtained by the agents via grid measurements.

Our preliminary results are encouraging and show the efficacy of this online and feedback optimization approach. These results will be detailed in a forthcoming submission.

## VI. CONCLUSIONS

In this paper we presented a geometric approach to the derivation of a linear approximant for the set of feasible power flows on a grid. The proposed approximant generalizes existing standard linear models, extends them to general linearization points and three phase networks, and is both sparse and structure-preserving. We illustrated the potential of the proposed model via a series of relevant applications, and we discussed some open questions regarding how to assess and possibly improve the quality of the approximation.

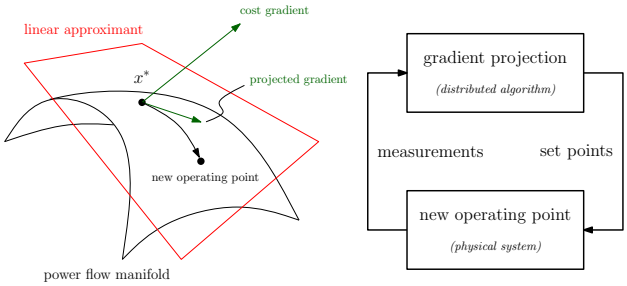


Fig. 8. Schematic representation of the iterative method proposed in Section V-D for the distributed solution of optimal power flow problems, based on the linear power flow manifold approximant proposed in Section III.

## APPENDIX

### A. Proof of Proposition 1

In order to simplify the derivation, we introduce an additional state corresponding to the *nodal injected currents* $i_h$ so that we can characterize feasible power flows via the implicit complex equations

$$Yu = i \tag{16}$$

$$\operatorname{diag}(u)\bar{i} = s. \tag{17}$$

Aside from simplifying the calculations, the current is also critical state in certain applications (e.g., thermal limits and protection), and it may be desirable to represent it explicitly.

By introducing the aggregate state vector $z = (v, \theta, \operatorname{Re} i, \operatorname{Im} i, p, q)$, we express (16) and (17) as

$$\mathbb{0}_{4n} = F(z) = \begin{bmatrix} F^{\text{grid}}(z) \\ F^{\text{bus}}(z) \end{bmatrix} = \begin{bmatrix} \operatorname{Re}(Yu-i) \\ \operatorname{Im}(Yu-i) \\ \operatorname{Re}(\operatorname{diag}(u)\bar{i}-s) \\ \operatorname{Im}(\operatorname{diag}(u)\bar{i}-s) \end{bmatrix},$$

where $F^{\text{grid}}$ and $F^{\text{bus}}$ are mappings from $\mathbb{R}^{6n}$ to $\mathbb{R}^{2n}$.

We obtain the voltage, current, and injection manifold

$$\mathcal{M} := \{z \in \mathbb{R}^{6n} \mid F(z) = \mathbb{0}_{4n}\}. \tag{18}$$

Let $z^*$ be such that $F^{\text{grid}}(z^*) = \mathbb{0}_{2n}$ and $F^{\text{bus}}(z^*) = \mathbb{0}_{2n}$. We compute the plane that is tangent to the manifold in $z^*$ as the subspace orthogonal to the rows of $\partial F/\partial z$ in $z^*$.

Before working out the explicit tangent plane, we briefly review how complex-valued functions and their derivatives can be expressed in real-valued coordinates. Adopting the notation in Proposition 1, observe that, if $x \in \mathbb{C}^n$ and we consider the function $f(x) := Ax$ as a *real-valued* function from $\mathbb{R}^{2n}$ to $\mathbb{R}^{2n}$, then we have that $\frac{\partial f}{\partial x} = \langle A \rangle$. Notice moreover that the the function $g(x) := \overline{x}$ satisfies $\partial g/\partial x = N$ and we have the identity $\langle \overline{A} \rangle = N\langle A \rangle N$. For ease of notation, we denote

$$\nu := \begin{bmatrix} v \\ \theta \end{bmatrix} \quad \text{and} \quad \iota := \begin{bmatrix} \operatorname{Re} i \\ \operatorname{Im} i \end{bmatrix}.$$

Notice that

$$\partial \begin{bmatrix} \operatorname{Re} u \\ \operatorname{Im} u \end{bmatrix} \Big/ \partial \begin{bmatrix} v \\ \theta \end{bmatrix} = R(u), \quad \text{and therefore} \quad \frac{\partial \cdot}{\partial \nu} = \frac{\partial \cdot}{\partial u} R(u).$$

With the above shorthands, we obtain

$$\frac{\partial F^{\text{grid}}}{\partial \nu} = \langle Y \rangle R(u) \qquad \frac{\partial F^{\text{grid}}}{\partial \iota} = -I \qquad \frac{\partial F^{\text{grid}}}{\partial s} = 0$$

$$\frac{\partial F^{\text{bus}}}{\partial \nu} = \langle \operatorname{diag} \bar{i} \rangle R(u) \qquad \frac{\partial F^{\text{bus}}}{\partial \iota} = \langle \operatorname{diag} u \rangle N \qquad \frac{\partial F^{\text{bus}}}{\partial s} = -I.$$

The complete Jacobian in $z^*$ is therefore

$$\begin{bmatrix} \frac{\partial F^{\text{grid}}}{\partial z}\Big|_{z^*} \\ \frac{\partial F^{\text{bus}}}{\partial z}\Big|_{z^*} \end{bmatrix} = \begin{bmatrix} \langle Y \rangle R(u^*) & -I & 0 \\ \langle \operatorname{diag} \overline{i^*} \rangle R(u^*) & \langle \operatorname{diag} u^* \rangle N & -I \end{bmatrix}.$$

The tangent plane is therefore defined as

$$\begin{bmatrix} \frac{\partial F^{\text{grid}}}{\partial z}\Big|_{z^*} \\ \frac{\partial F^{\text{bus}}}{\partial z}\Big|_{z^*} \end{bmatrix} (z - z^*) = 0.$$

By eliminating the variables corresponding to the nodal currents, we obtain the result (4) in Proposition 1.

### B. Proof of Lemma 1

According to the statement of Proposition 1, the gradient $\partial F / \partial x$ of defining function $F : \mathbb{R}^{4n} \to \mathbb{R}^{2n}$ is surjective, as it has constant full rank $2n$. $F$ is therefore a submersion, and according to [29, Corollary 8.9 (Submersion Level Set Theorem)] the level set of a submersion is an embedded $2n$-dimensional submanifold.

### C. Proof of Proposition 2

Let us introduce a function $h(\alpha)$ defined as

$$h(\alpha) = F_i(x^* + \alpha(x - x^*)).$$

The function $h$ returns the value of $F_i$ on the line segment that connects $x^*$ on the manifold $\mathcal{M}$ (for $\alpha = 0$) to a point $x$ on the tangent space of $\mathcal{M}$ at $x^*$ (for $\alpha = 1$), and admits a Taylor expansion in $\alpha = 0$. We therefore have

$$h(\alpha) = h(0) + \alpha\, h'(\alpha)\big|_{\alpha=0} + \frac{\alpha^2}{2}\, h''(\alpha)\big|_{\alpha=\beta},$$

where $\beta \in [0, \alpha]$. Using the fact that

$$h'(\alpha) = \frac{\partial F_i}{\partial x}\bigg|_{x^* + \alpha(x - x^*)} (x - x^*)$$
$$h''(\alpha) = (x - x^*)^T \frac{\partial^2 F_i}{\partial x^2}\bigg|_{x^* + \alpha(x - x^*)} (x - x^*),$$

we obtain

$$h(\alpha) = F_i(x^*) + \alpha \frac{\partial F_i}{\partial x}\bigg|_{x^*} (x - x^*) + \frac{\alpha^2}{2}(x - x^*)^T \frac{\partial^2 F_i}{\partial x^2}\bigg|_{x^* + \beta(x - x^*)} (x - x^*).$$

Finally, by using the fact that $\epsilon_i(x) = F_i(x) = h(1)$, and by using the fact that $F_i(x^*) = 0$ and $\frac{\partial F_i}{\partial x}\Big|_{x^*} (x - x^*) = 0$ (because $x$ belongs to the tangent plane), we have

$$\epsilon_i(x) = \frac{1}{2}(x - x^*)^T \frac{\partial^2 F_i}{\partial x^2}\bigg|_{x^* + \beta(x - x^*)} (x - x^*).$$

If $\left\| \frac{\partial^2 F_i}{\partial x^2} \right\| \leq B_i$ for all $x \in \mathcal{B}(x^*, \delta)$, then

$$|\epsilon_i| \leq \frac{B_i}{2} \|x - x^*\|^2.$$

## ACKNOWLEDGMENT

The authors thank Sandro Zampieri, Bing Li, Giovanni Sansavini, Dalibor Drzajic, Adrian Hauswirth, and Gabriela Hug, for the useful discussion and the relevant comments.

## REFERENCES

[1] L. Xie, D.-H. Choi, S. Kar, and H. Poor, "Fully distributed state estimation for wide-area monitoring systems," *IEEE Trans. on Smart Grid*, vol. 3, no. 3, Sep. 2012.
[2] V. Kekatos and G. B. Giannakis, "Distributed robust power system state estimation," *IEEE Trans. on Power Systems*, vol. 28, no. 3, 2013.
[3] O. Vukovic, K. C. Sou, G. Dan, and H. Sandberg, "Network-aware mitigation of data integrity attacks on power system state estimation," *IEEE J. on Selected Areas in Comm.*, vol. 30, no. 6, Jul. 2012.
[4] F. Pasqualetti, F. Dörfler, and F. Bullo, "Attack detection and identification in cyber-physical systems," *IEEE Trans. on Autom. Control*, vol. 58, no. 11, 2013.
[5] O. Sundström and C. Binding, "Flexible charging optimization for electric vehicles considering distribution grid constraints," *IEEE Trans. on Smart Grids*, vol. 3, no. 1, Mar. 2012.
[6] I. A. Hiskens, "Analysis tools for power systems-contending with nonlinearities," *Proc. of the IEEE*, vol. 83, no. 11, 2002.
[7] J. C. Willems, "Terminals and ports," *IEEE Circuits and Systems Magazine*, vol. 10, no. 4, pp. 8–26, 2010.
[8] D. Deka, S. Backhaus, and M. Chertkov, "Structure learning in power distribution networks," *arXiv preprint arXiv:1501.04131*, 2015.
[9] S. V. Dhople, S. S. Guggilam, and C. Y. Chen, "Linear approximations to AC power flow in rectangular coordinates," in *Allerton Conf.*, 2015.
[10] S. Bolognani and S. Zampieri, "On the existence and linear approximation of the power flow solution in power distribution networks," *IEEE Trans. on Power Systems*, to appear in 2015. arXiv:1403.5031.
[11] B. Stott, J. Jardim, and O. Alsaç, "DC power flow revisited," *IEEE Trans. on Power Systems*, vol. 24, no. 3, Aug. 2009.
[12] B. Gentile, J. W. Simpson-Porco, F. Dörfler, S. Zampieri, and F. Bullo, "On reactive power flow and voltage stability in microgrids," in *American Control Conference (ACC)*, 2014.
[13] M. E. Baran and F. F. Wu, "Network reconfiguration in distribution systems for loss reduction and load balancing," *IEEE Trans. on Power Delivery*, vol. 4, no. 2, pp. 1401–1407, Apr. 1989.
[14] M. Farivar, L. Chen, and S. Low, "Equilibrium and dynamics of local voltage control in distribution systems," in *IEEE CDC*, 2013.
[15] N. Li, G. Qu, and M. Dahleh, "Real-time decentralized voltage control in distribution networks," in *IEEE Allerton Conf.*, 2014.
[16] S. Bolognani, "1ACPF - First-order AC power flow model," GitHub, 2015. [Online]. Available: http://github.com/saveriob/1ACPF
[17] K. Turitsyn, P. Šulc, S. Backhaus, and M. Chertkov, "Options for control of reactive power by distributed photovoltaic generators," *Proc. IEEE*, vol. 99, no. 6, pp. 1063–1073, Jun. 2011.
[18] M. Chen, "On the solution of circulant linear systems," *SIAM J. Numer. Anal.*, vol. 24, no. 3, Jun. 1987.
[19] C. F. Wagner and D. E. Robert, *Symmetrical components as applied to the analysis of unbalanced electrical circuits*. McGraw-Hill, 1933.
[20] W. H. Kersting, "Radial distribution test feeders," in *IEEE PES Winter Meeting*, vol. 2, Jan. 2001, pp. 908–912.
[21] S. Bolognani and F. Dörfler, "Fast scenario-based decision making in unbalanced distribution networks," in *Power Systems Computation Conference (PSCC)*, submitted.
[22] G. C. Calafiore and M. C. Campi, "The scenario approach to robust control design," *IEEE Trans. on Autom. Control*, vol. 51, no. 5, 2006.
[23] D. Drzajic, "Energy theft detection using compressive sensing methods," ETH Zürich, Semester project report, 2015.
[24] E. Zio and G. Sansavini, "Component criticality in failure cascade processes of network systems," *Risk Analysis*, vol. 31, no. 8, 2011.
[25] J. Chen, J. S. Thorp, and I. Dobson, "Cascading dynamics and mitigation assessment in power system disturbances via a hidden failure model," *Intl. J. of Electrical Power and Energy Syst.*, vol. 27, no. 4, May 2005.
[26] B. Li, G. Sansavini, S. Bolognani, and F. Dörfler, "Operations and cascading outages dynamic model based on linear AC power flow," working paper.
[27] D. Gabay, "Minimizing a differentiable function over a differential manifold," *J. of Optim. Theory and Applic.*, vol. 37, no. 2, Jun. 1982.
[28] P.-A. Absil, R. Mahony, and R. Sepulchre, *Optimization algorithms on matrix manifolds*. Princeton University Press, 2008.
[29] J. M. Lee, "Smooth manifolds," in *Introduction to Smooth Manifolds*. Springer New York, 2003, vol. 218, pp. 1–29.